JACS Au
AN OPEN ACCESS JOURNAL OF THE AMERICAN CHEMICAL SOCIETY

pubs.acs.org/jacsau

Article

Inhomogeneity Effects on Reactions in Supercritical Fluids: A Computational Study on the Pyrolysis of *n*-Decane

Yutong Wang and Guozhu Liu*

Cite This: *JACS Au* 2022, 2, 2081−2088

Read Online

ACCESS | Metrics & More | Article Recommendations | Supporting Information

ABSTRACT: Supercritical fluids exhibit peculiar inhomogeneity, which strongly affects reaction behaviors in them. However, explanations for inhomogeneity and its effect on reactions are both ambiguous so far. Here, we provide an atomic-level understanding of inhomogeneity effects on reactions via the computational method, with the example of *n*-decane pyrolysis under supercritical conditions. We describe the characteristic pyrolysis behaviors through collective variable-driven hyperdynamics (CVHD) simulations and explain the inhomogeneity of supercritical *n*-decane as the coexistence of gas-like and liquid-like atoms by a trained machine learning classifier. Due to their specific local environment, the appearance of liquid-like atoms under supercritical conditions significantly increases the type and frequency of bimolecular reactions and eventually causes changes in product distributions. Future research with this method is expected to extend the effect of inhomogeneity on other reactions under supercritical conditions or other condensed phases.

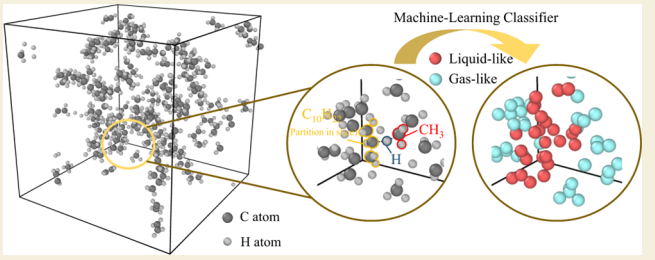

KEYWORDS: *supercritical, pyrolysis, n-decane, hyperdynamics, machine learning*

INTRODUCTION

Supercritical fluids acting as solvents, media, and reactants have been applied in many chemical and engineering applications. This is attributable primarily to reactions under supercritical conditions that frequently possess unexpected behaviors, including products, mechanisms, and rates.[1−4] Taking pyrolysis, the essential process during the utilization of fossil energy as an example, mass experiments have reported that the hydrocarbon pyrolysis chemistry under supercritical conditions is quite different from that under atmospheric conditions, which visually manifests in marked changes in product compositions.[5−7] While there exist rich potential applications of reactions under supercritical conditions, the realization of this potential is severely hindered due to the lack of in-depth knowledge of these reaction behaviors.

A significant effort has been committed to revealing the reason for peculiar reaction behaviors under supercritical conditions and attributes it to the characteristics of supercritical fluids, i.e., the inhomogeneity in spatial scale.[8,9] However, this inhomogeneity itself remains elusive. Earlier, researchers vividly describe the inhomogeneity as "clustering" or "solvation": when solute molecules are positioned in supercritical fluid, other solvent molecules will gather around solute molecules.[10,11] Further experiments indicate that due to this clustering, reactions under supercritical conditions display a cage effect.[12,13] However, the terminology "clustering" itself can cause much controversy since clustering may come from the solute-induced density enhancement or the density fluctuation of supercritical fluid.[14] Recent progress in molecular dynamics (MD) simulations on Lennard-Jones (LJ) fluids in conjunction with the Voronoi tessellation provides us atomic-level insights to reconcile conflicting hypotheses and to understand the microstructure of supercritical fluid. The result suggests that no distinct cluster exists.[15,16] Subsequent machine learning analysis on simulation data allows a direct classification of liquid-like and gas-like particles coexisting in the supercritical LJ fluid and provides a microscopic view of the supercritical fluid as a mixture of liquid-like and gas-like structures.[17,18]

The above description of inhomogeneity has been implemented at the atomic level. However, a commensurate description of reactions goes beyond the ability of traditional experiments. Several recently proposed techniques such as molecular beam sampling (MBS) and synchrotron vacuum ultraviolet photoionization mass spectrometry (SVUV-PIMS) provide important experimental methods to trap and identify the special intermediates and products with sufficient accuracy.[19−21] With these methods, the increased production of biphenyl radicals is identified during hexane and benzene

Received: June 19, 2022
Revised: August 24, 2022
Accepted: August 24, 2022
Published: September 6, 2022

https://doi.org/10.1021/jacsau.2c00359
JACS Au 2022, 2, 2081−2088

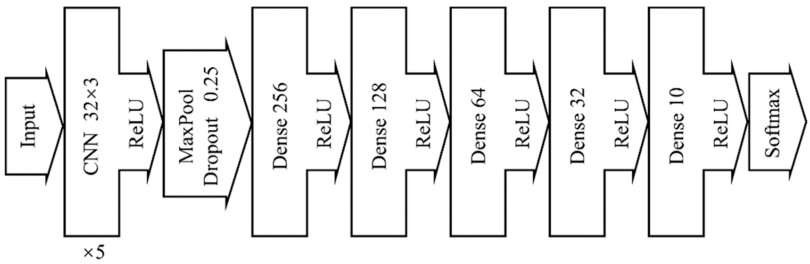

Figure 1. Architecture of DNN trained in this work.

pyrolysis under supercritical conditions.[22] Although such sampling methods provide in situ reaction analysis, they do not provide a complete description of the inhomogeneous distribution of atoms under supercritical conditions. Thus, product distributions mentioned above are therefore speculatively interpreted as the enhancement of bimolecular reactions due to supercritical clustering.[23] To alleviate this drawback, reactive MD simulation is adopted as an alternative computational method. Reactive MD simulation has the capability of identifying key intermediate radicals and reaction pathways, meanwhile providing a dynamic description of particle distributions.[24] There have been mass successful applications of reactive MD simulations on reactions under supercritical conditions.[25−28] Furthermore, with an unprecedentedly long time scale of simulations achieved by hyperdynamics paradigms, detailed reaction dynamics under experimentally realistic conditions can be verified through direct simulations.[29−31] These state-of-the-art in silico simulation methods grant us access to an integrative explanation of anomalous behaviors and a linkage between anomalies and reactions under supercritical conditions.

This work seeks to interpret the inhomogeneity of neat supercritical fluids and how it may affect reactions under supercritical conditions with the computational method. The pyrolysis of *n*-decane is chosen as the prototype due to its representative role in advanced fuel systems, which usually operate under supercritical conditions. Meanwhile, previous research has pointed out that pyrolysis kinetic models under gas conditions are unable to calibrate reactions under supercritical conditions.[32−34] Here, we first describe the reaction dynamics of pyrolysis under supercritical conditions by collective variable-driven hyperdynamics (CVHD) simulations, highlighting the mainstream reactions associated with stable species. A machine learning classifier is adopted to stratify distinct liquid-like and gas-like atoms coexisting in supercritical *n*-decane. The effects of liquid-like atoms on reactions are also discussed, focusing on the promotion of bimolecular reactions. Albeit further perfection is needed, the present study sheds light on reactions of practical working fluids under supercritical conditions and, what's more, in the sense that the proposed methods can be extended to analogous reactions under supercritical conditions.

METHODS

MD Simulations

Nonreactive MD simulations are performed using Large-scale Atomic/Molecular Massively Parallel Simulator (LAMMPS) software, version 64-bit 8Feb2019.[35,36] The system energy is calculated using all-atom optimized potentials for liquid simulation (OPLS-AA) forcefield due to its satisfactory outcome of modeling supercritical hydrocarbons.[37] Forcefield parameters, equations of the system energy, and mixing rules are directly excerpted from the original literatures with only *pro-forma* corrections for the compatibility of LAMMPS's input file.[38] Initial simulation system encompasses 300 *n*-decane molecules placed in a periodic cubic box. The system takes the following process: minimization, annealing reorientation under a high temperature of 1300 K, and then equilibration under the required temperature of 400 ps. The production run is carried out for 100 ps, whose trajectories are used to compute bulk density and perform Voronoi tessellations. The remaining simulation parameters maintain the same as the settings of our previous simulations on supercritical JP-10 and thus are not repeated here.[39]

CVHD simulations are performed using the ReaxFF modeling suite of Amsterdam Density Functional (ADF) software.[40] The system energy is calculated using the ReaxFF CHO-2016 forcefield.[41] Transferability of the adopted forcefield has been well demonstrated by applications to pyrolysis and combustion of different hydrocarbons, such as cyclohexanone and JP-10.[42,43] More descriptions of the formalism can be found in previous literatures about ReaxFF.[44] The incorporated ChemTraYzer (CTY) module of ADF software, together with the individual ReacNetGenerator (RNG) package, is selected to process simulation trajectories.[45] The initial system consists of 25 *n*-decane molecules randomly placed in the cubic box, whose dimension is adjusted to produce the required densities (0.01 and 0.15 g/cm^3). The prepared system is then simulated through NVT (isochoric−isothermal) simulations at 1000 K, and the Nosé−Hoover chain with a damping constant of 100 fs is used to control the temperature. After minimization, the production run was 2×10^8 steps with a time step of 0.1 fs. The density of 0.01 and 0.15 g/cm^3 at 1000 K corresponds to gas and supercritical conditions separately (approximately 0.1 and 8.4 MPa). The C−H and C−C bond lengths are chosen as the collective variable (CV). R_{min} and R_{max} are 1.05 and 1.65 Å for the C−H bonds, while they are 1.55 and 2.20 Å for the C−C bonds. Gaussian bias with a height of 0.25 kcal/mol and a delta of 0.025 is built with a deposition frequency of 2000 steps. The waiting time for reaction declaration is 10,000 steps. The applicability and validation of CVHD in our simulation system can be found in the Supporting Information. Unless otherwise stated, all results are calculated with the average or statistic of four independent trajectories to minimize the statistical uncertainty, and the comparisons between different conditions are made at a fixed conversion of approximately 50%.

Machine Learning

A deep neural network (DNN) is trained to label the liquid-like and gas-like atoms in supercritical *n*-decane. As shown in Figure 1, the architecture is designed based on the network of Ha et al., which has shown excellent performance in labeling the liquid-like and gas-like particles in the supercritical LJ fluid.[17] Considering the local environment of atoms in *n*-decane, the sample in data set is an $(N + 1) \times 4$ array encompassing features of the center atom and its N nearest neighbors. Features include the distance to the center atom, atom type, Voronoi density, and number of Voronoi neighbors, of which the Voronoi tessellation of MD trajectory is performed by the Voro++ library.[46] Details on the training are provided in the Supporting Information, including the generation of data set, the iteration of N, and the evaluation of model.

https://doi.org/10.1021/jacsau.2c00359
JACS Au 2022, 2, 2081−2088

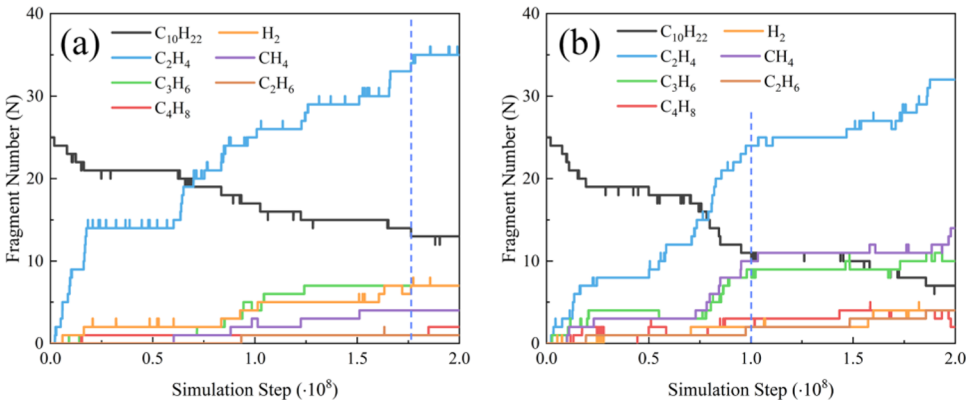

Figure 2. Typical time-dependent evolution of *n*-decane and main product fragments during simulation under (a) gas conditions and (b) supercritical conditions (the blue dashed line indicates that 50% conversion of *n*-decane is reached).

RESULTS AND DISCUSSION

Enhanced Production of Alkanes

CVHD simulations are performed under both gas and supercritical conditions, aiming at the comparison of reaction products and pathways. Figure 2a,b shows the typical evolution of the main species versus simulation steps. Products observed under two different conditions are generally consistent. The initial decomposition of *n*-decane is accompanied by the massive formation of alkene products, indicating that alkenes are primary pyrolysis products. In addition, Figure 2b also indicates a significant enhancement in the yield of alkanes under supercritical conditions, especially in the later stage of simulation. To further illustrate, Figure 3 shows the amount of

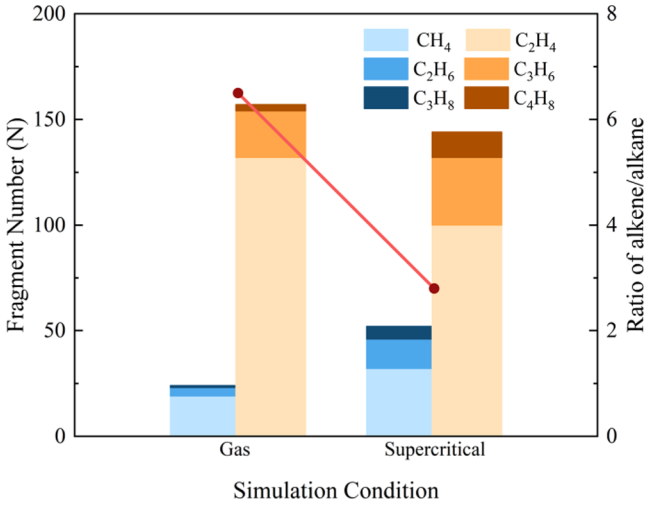

Figure 3. Fragment numbers (left axis) and ratio (right axis) of main alkane and alkene products under different conditions.

main alkane and alkene products severally. Under gas conditions, alkenes are dominant, while alkanes only comprise about 15% of products. This product distribution is similar to Malewicki et al.'s experimental results under low partial pressure.[47] In contrast, the supercritical condition gives rise to the increase of alkane products, which is reified as the decrease of alkene/alkane ratio from 6.5 to 2.8. Such a distribution is closer to Jia et al.'s experimental results under supercritical conditions.[32] It should be noted that the supercritical condition yields larger (C2 and higher) products, which is also referred in our previous experimental studies.[34]

Favored Bimolecular Reactions

Diverse product distributions indicate that reaction mechanisms under gas and supercritical conditions are different. To further understand the characteristic pyrolysis dynamics, detailed reaction networks are proposed under gas and supercritical conditions in Figures S6 and S7. To explicate complex networks, we here discuss reaction pathways associated with typical stable species. As shown in Figure 4a, consumption channels of *n*-decane involve mainly H-abstraction and C−C bond dissociation, but the proportion of two channels changes with conditions. Under gas conditions, H-abstraction consumes 66% of *n*-decane, while this proportion increases to 82% under supercritical conditions. We further detailed the contributions of different radicals involved in H-abstraction reactions, as shown in Figure 4b. Under gas and supercritical conditions, H-abstraction by the H radical contributes 53 and 15% to the consumption of *n*-decane, while the CH_3 radical contributes 32 and 56%, respectively. Furthermore, additional larger radicals such as C_3H_7 and C_4H_9 are detected to participate in H-abstraction reactions under supercritical conditions.

In addition to the initial consumption of *n*-decane, more products are generated via subsequent reactions of various intermediates. Here, we list the formation channels of the main stable products in Figure 5a−f. As shown in Figure 5a−c, most alkenes are mainly formed through two unimolecular reaction pathways, namely, the β-C−C scission and β-C−H scission of different radicals generated from initial consumptions of *n*-decane and subsequent decomposition reactions. Under gas conditions, the β-C−C scission forms 70% C_2H_4, and this proportion increases to 80% under supercritical conditions. However, the corresponding reaction net flux decreases due to isomerization reducing the number of 1-radicals. It should also be noted that some bimolecular reactions are observed under supercritical conditions, namely, the recombination such as C_3H_5 and CH_3, which contributes over 10% to the formation of C_4H_8. The primary formation pathway for alkanes is bimolecular H-abstraction, as shown in Figure 5d−f. H-abstraction with CH_3 forms all CH_4, of which 55 and 62% are formed from *n*-decane under gas and supercritical conditions, respectively. Fragments with lower carbon number, such as C_2H_4 and C_2H_5, also take part in the formation of CH_4. Similarly, the H-abstraction of C_2H_5 and C_3H_7 is the principal

https://doi.org/10.1021/jacsau.2c00359
JACS Au 2022, 2, 2081−2088

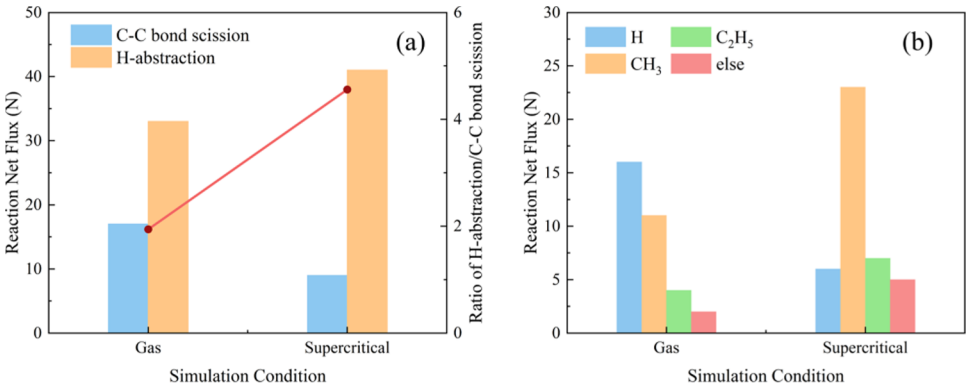

Figure 4. Reaction net flux of (a) the initial decomposition channels and (b) initial H-abstraction reactions with different radicals of *n*-decane pyrolysis under different simulation conditions.

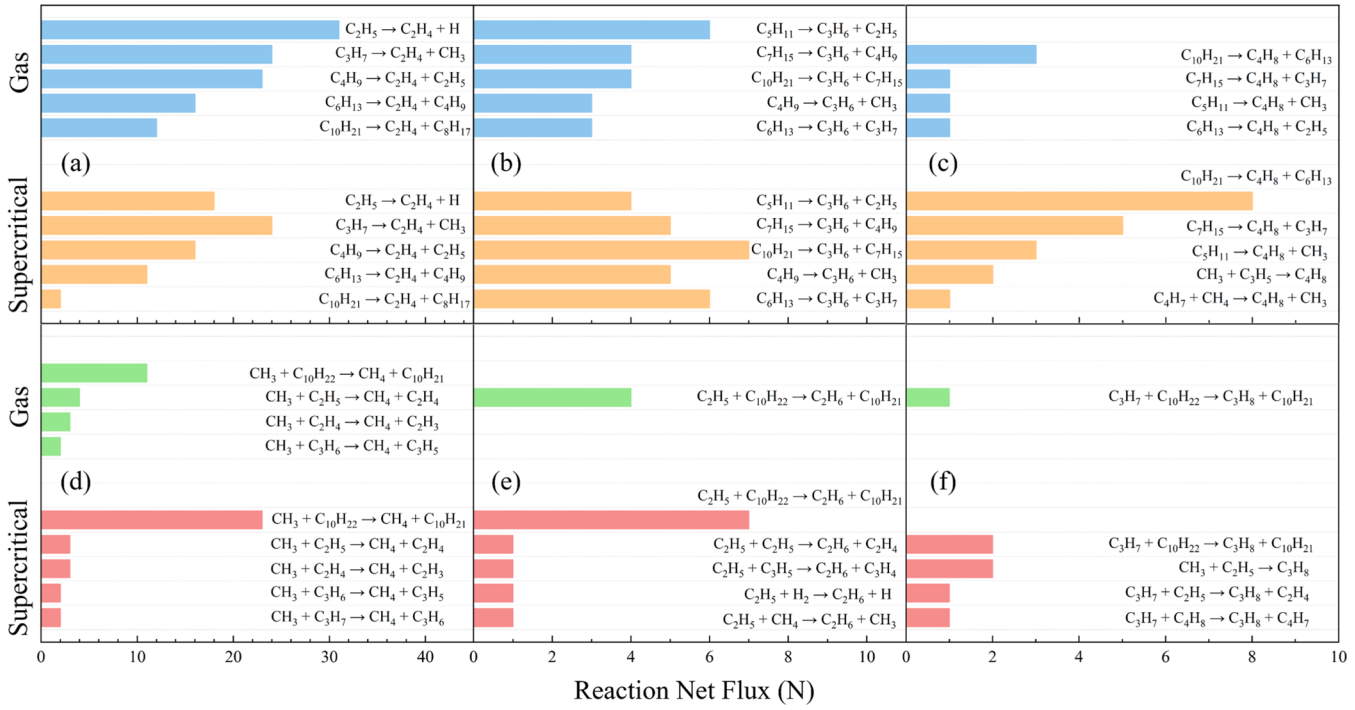

Figure 5. Reaction net flux of the formation channel of stable product. (a) C_2H_4, (b) C_3H_6, (c) C_4H_8, (d) CH_4, (e) C_2H_6, and (f) C_3H_8.

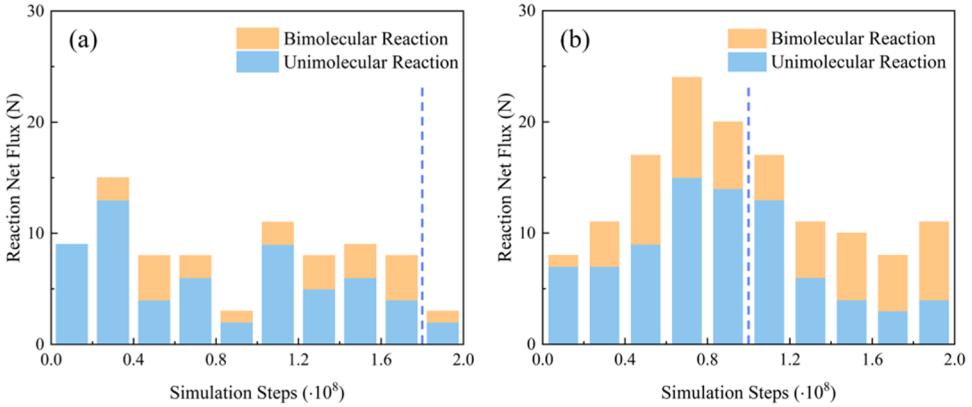

Figure 6. Time-dependent evolution of unimolecular and bimolecular reactions during *n*-decane pyrolysis under (a) gas conditions and (b) supercritical conditions (the blue dashed line indicates that 50% conversion of *n*-decane is reached).

formation channel of C_2H_6 and C_3H_8. Besides, the bimolecular recombination of alkyl radicals such as CH_3 and C_2H_5 becomes another important pathway of larger alkanes under supercritical conditions. Same as the recombination forming

https://doi.org/10.1021/jacsau.2c00359
JACS Au 2022, 2, 2081−2088

alkenes, such a bimolecular reaction is quite common in previous experimental mechanisms for the alkane formation, while rarely mentioned in previous simulations under gas conditions, especially under high-temperature conditions.[34]

Compared to the reaction mechanism itself, the difference between mechanisms under gas and supercritical conditions concerns us more. Previous studies supposed that the pressure affects product distribution by adjusting the relative importance of unimolecular and bimolecular reactions.[22] The same conclusion also emerges from the discussion above. We further plot time-dependent evolutions of unimolecular and bimolecular reactions detected in simulations under gas and supercritical conditions in Figure 6. Unimolecular reactions mainly concentrate in the early stage of the reaction, while the bimolecular reaction gradually increases in the later stage. Figure 7 quantitatively characterizes the total unimolecular and bimolecular reactions, together with their ratio. The supercritical condition promotes the unimolecular and bimolecular reactions at the same time; however, the facilitation of the bimolecular reaction is more significant. In conclusion, we confirm the characteristic pyrolysis dynamics under supercritical conditions as the promotion of bimolecular reactions, which leads to the increase of alkane in products.

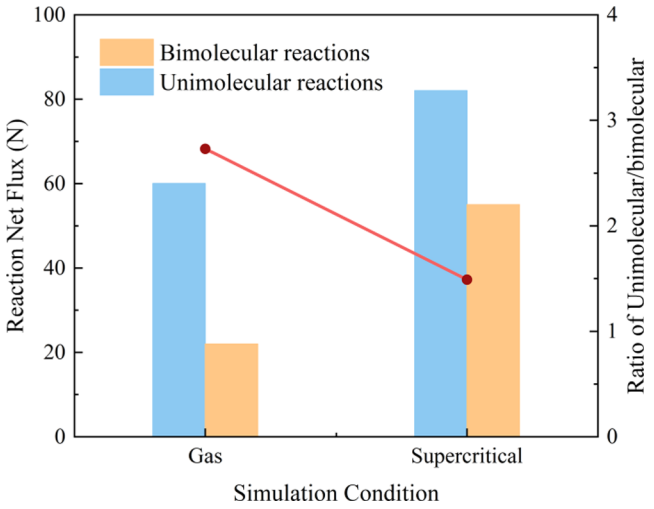

Figure 7. Reaction numbers (left axis) and ratio (right axis) of unimolecular and bimolecular reactions under different conditions.

Inhomogeneity of Supercritical *n*-Decane

To gain deeper insights into the promotion of bimolecular reactions under supercritical conditions, we should first clarify the characteristics of supercritical fluids. Supercritical fluids are known to exhibit inhomogeneous molecular distribution. We noted that our previous research has applied a statistical model based on the unit of molecules to examine the inhomogeneity of supercritical JP-10 and divided simulation systems into coarse-grained liquid-like or gas-like regions.[39] However, when it comes to the above-mentioned reactions associated with one or several sets of atoms, a particle-based classification becomes necessary. In pursuit of this goal, our machine learning classifier is employed to label atoms in supercritical fluids as liquid-like or gas-like atoms, aiming at an atomic-level understanding of the inhomogeneity of supercritical *n*-decane.

Representative labeled snapshots are displayed in Figure 8, in which liquid-like and gas-like atoms form the inhomogeneous coexistence region: a foam-like structure encompasses intertwined clusters, which are neither phase-separated nor uniformly mixed. It is also clear that the proportion of liquid-like atoms changes with different conditions. Thus, the proportion of liquid-like atoms under different conditions (listed in Table S2) along the isothermal line of 1000 K is collected and shown in Figure 9. The proportion of liquid-like

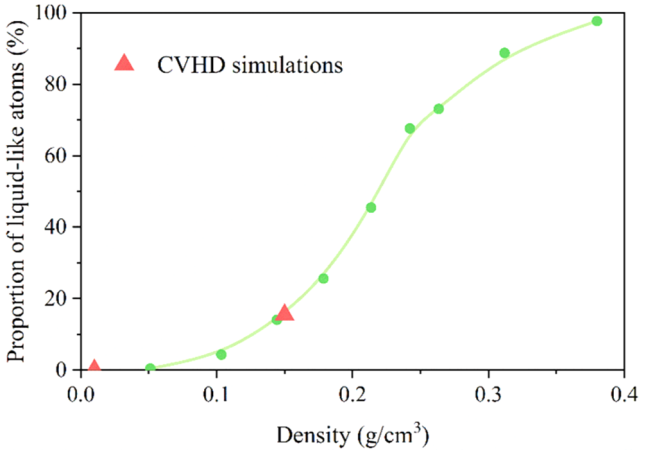

Figure 9. Proportion of liquid-like atoms in supercritical *n*-decane under different conditions along the isothermal line of 1000 K (green circles denote the classification of nonreactive MD simulations, while the green line is the corresponding fitting curve. Red triangles denote the classification of CVHD simulations).

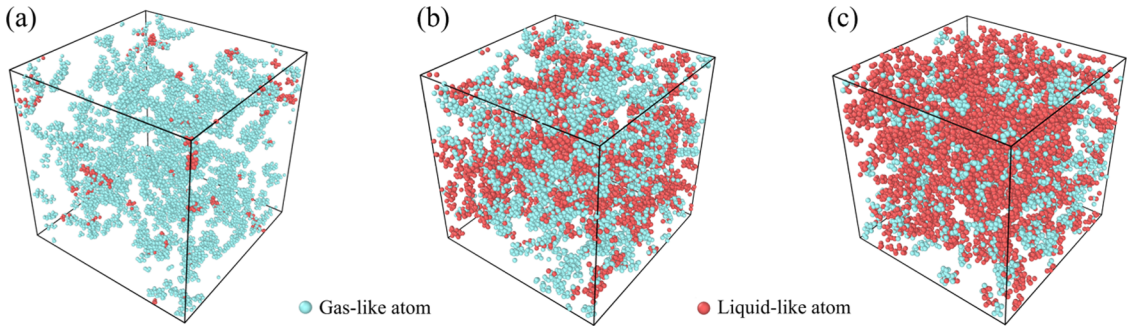

Figure 8. Representative labeled snapshots of supercritical *n*-decane at (a) 3 MPa, (b) 15 MPa, and (c) 30 MPa (derived from nonreactive MD simulations).

https://doi.org/10.1021/jacsau.2c00359
JACS Au 2022, 2, 2081−2088

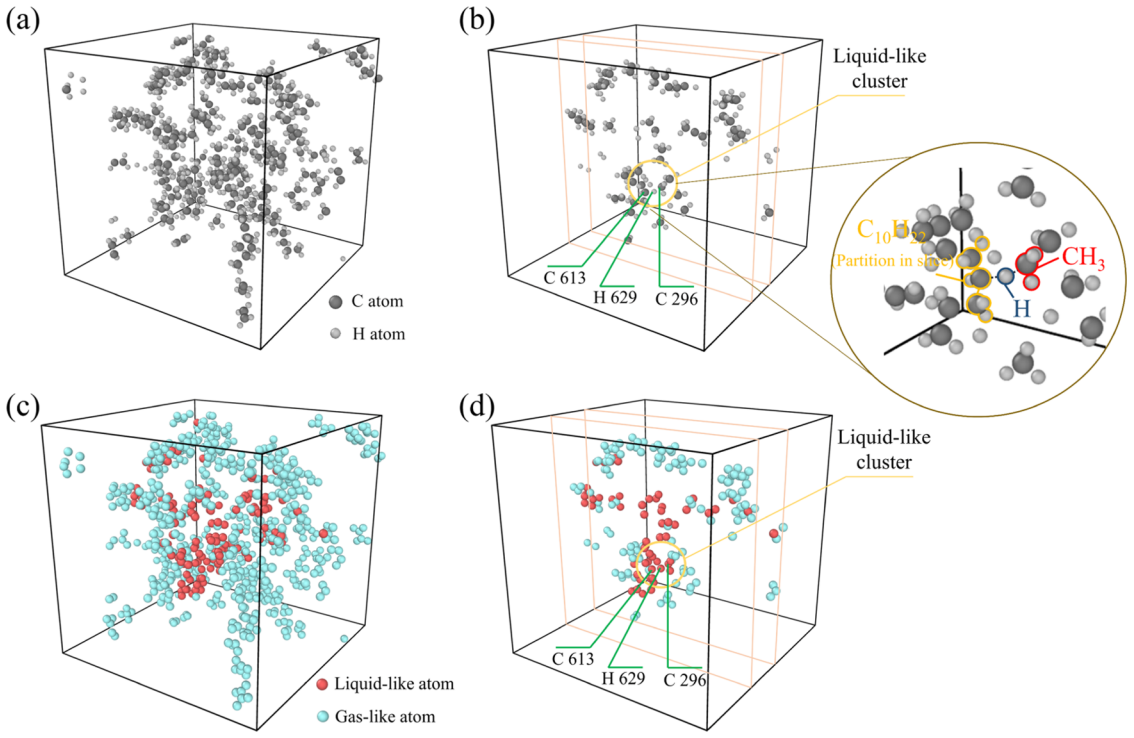

Figure 10. Representative snapshots of supercritical *n*-decane: (a) unlabeled snapshot containing the detected reaction. (b) Slice of the unlabeled snapshot containing the detected reaction. (c) Labeled snapshot containing the detected reaction. (d) Slice of the labeled snapshot containing the detected reaction (derived from CVHD simulations).

atoms in supercritical *n*-decane increases with an increasing pressure or, more specific, the increasing bulk density. In addition, the variation tendency of proportion fits the sigmoidal curve, which closely resembles the results of the LJ supercritical fluid.[17] This suggests that the existence of liquid-like atoms in hydrocarbons also depends on bulk properties, even if the hydrocarbons behave far from ideal models. We also label atoms in CVHD simulations, and the average results in Figure 9 (Red triangles) show good agreement with the isothermal fitting curve, proving the existence of liquid-like atoms in supercritical *n*-decane described by CVHD simulation with reactions. This further demonstrates the portability of the machine learning classifier between different forcefields, which is considered the indispensable linkage of inhomogeneity and the following analysis of reactions.

Liquid-Like Atoms and Bimolecular Reactions

Classifications by the machine learning classifier demonstrate that inhomogeneity, interpreted as the mixture of liquid-like and gas-like atoms, serves as an atomic-level hallmark of supercritical *n*-decane. Imagine that the reaction system switches from gas condition to supercritical condition along the isotherm line shown in Figure 9; then, the most significant variation is the appearance and increase of liquid-like atoms. Meanwhile, the number of bimolecular reactions also increases, then leading to the characteristics of supercritical pyrolysis. To clarify this ambiguous relation, we randomly select 20 sets of bimolecular reactions detected in the CVHD simulations and label the system snapshots containing detected reactions with our trained machine learning classifier. For further illustration, the visualization results of one reaction ($CH_3 + C_{10}H_{22} \rightarrow CH_4 + C_{10}H_{21}$) are shown in Figure 10. Here, we define the reaction site as three atoms directly related to the reaction, for example, C296 in CH_3, C613 in $C_{10}H_{22}$, and H629 in $C_{10}H_{22}$. For the reaction, we take as an example all three reaction sites as liquid-like atoms. Further, this bimolecular reaction takes place in a liquid-like region consisting mostly of liquid-like atoms. Table S4 lists the label of reaction sites of 20 bimolecular reactions. Seventy percent of sampled reactions have more than one liquid-like reaction site, with 50% of them having all three reaction sites as liquid-like. Considering that the proportion of liquid-like atoms in the whole system is only 15% under the simulation condition, yet liquid-like atoms are present in 70% of bimolecular reactions. This result demonstrates the appearance of liquid-like atoms, i.e., the inhomogeneity is the main distinguishing factor for reactions under supercritical conditions when compared to reactions under gas conditions. Analogous to atoms in the real liquid phase, the liquid-like atoms sharing a similar local environment mean high local density, which benefits the bimolecular effective collisions and the occasion of subsequent bimolecular reactions.[48,49] In general, the effect of supercritical inhomogeneity on pyrolysis is mainly manifested by the appearance and increase of liquid-like atoms, favoring bimolecular reactions and finally leading to the characteristic of pyrolysis under supercritical conditions relative to gas conditions.

CONCLUSIONS

In this study, the inhomogeneity of supercritical *n*-decane and its effect on the supercritical pyrolysis under typical working conditions are systematically investigated. The CVHD method enables an extraordinary time scale of our simulations, which unravel the characteristic of supercritical pyrolysis, while the machine learning classifier allows us to obtain a dynamic description of supercritical *n*-decane at the atomic level and then label the liquid-like and gas-like atoms involved.

https://doi.org/10.1021/jacsau.2c00359
JACS Au 2022, 2, 2081−2088

Supercritical *n*-decane shows a foam-like structure encompassing the inhomogeneous intertwined coexistence of liquid-like atoms and gas-like atoms. These unique liquid-like atoms only appear under supercritical conditions, and it is also found that the proportion of liquid-like atoms in the supercritical *n*-decane system falls directly under the sway of bulk density. Due to the differences in the local environment of liquid-like and gas-like atoms, the appearance of liquid-like atoms makes prominent distinctions between reaction behaviors under gas conditions and supercritical conditions. Benefitting from the local environment of liquid-like atoms, bimolecular reactions such as H-abstraction and recombination of alkyl radicals take more favorable positions under supercritical conditions, lead to the formation of more heavy alkanes, and then eventually form the specific product distribution. Based on the concept of liquid-like atoms, the current report proposes an interpretation for the particularity of supercritical pyrolysis, which is expected to be suitable for other reactions under supercritical conditions or other condensed phases. While further development of correlation between liquid-like atoms and bimolecular reactions in terms of spatial and temporal scales is still needed, related research is currently being carried out in our group.

■ ASSOCIATED CONTENT

Supporting Information

The Supporting Information is available free of charge at https://pubs.acs.org/doi/10.1021/jacsau.2c00359.

Detailed information on the application and validation of the CVHD method, the training process of DNN, and the generation of training data set; the data required to reproduce these findings are all available from the corresponding authors upon request (PDF)

■ AUTHOR INFORMATION

Corresponding Author

Guozhu Liu − *Key Laboratory for Green Chemical Technology of Ministry of Education, School of Chemical Engineering and Technology, Tianjin University, Tianjin 300072, China; Haihe Laboratory of Sustainable Chemical Transformations, Tianjin 300192, China; Zhejiang Institute of Tianjin University, Ningbo, Zhejiang 315201, China;* orcid.org/0000-0003-2193-5289; Phone: +86-22-85356099; Email: gliu@tju.edu.cn

Author

Yutong Wang − *Key Laboratory for Green Chemical Technology of Ministry of Education, School of Chemical Engineering and Technology, Tianjin University, Tianjin 300072, China*

Complete contact information is available at: https://pubs.acs.org/10.1021/jacsau.2c00359

Author Contributions

The manuscript was written through contributions of all authors. The authors declare no competing financial interest. CRediT: **Yutong Wang** formal analysis, investigation, methodology, software, validation, visualization, writing-original draft; **Guozhu Liu** conceptualization, data curation, funding acquisition, project administration, supervision, writing-review & editing.

Notes

The authors declare no competing financial interest.

■ ACKNOWLEDGMENTS

The authors are grateful for the funding support of the National Natural Science Foundation of China [grant number 22025802]. The authors are also grateful to Prof. You Han (School of Chemical Engineering & Technology, Tianjin University, Tianjin 300072, China) for valuable discussion and suggestions on calculation.

■ ABBREVIATIONS

MD	molecular dynamics
LJ	Lennard-Jones
MBS	molecular beam sampling
SVUV-PIMS	synchrotron vacuum ultraviolet photoionization mass spectrometry
CVHD	collective variable-driven hyperdynamics
LAMMPS	Large-scale Atomic/Molecular Massively Parallel Simulator
OPLS-AA	all-atom optimized potentials for liquid simulations
ADF	Amsterdam Density Functional
CTY	ChemTraYzer
RNG	ReacNetGenerator
NVT	isochoric−isothermal
DNN	deep neural network

■ REFERENCES

(1) Eckert, C. A.; Knutson, B. L.; Debenedetti, P. G. Supercritical fluids as solvents for chemical and materials processing. *Nature* **1996**, *383*, 313−318.

(2) Brunner, G. Applications of Supercritical Fluids. *Annu. Rev. Chem. Biomol. Eng.* **2010**, *1*, 321−342.

(3) Knez, Ž.; Markočič, E.; Leitgeb, M.; Primožič, M.; Knez Hrnčič, M.; Škerget, M. Industrial applications of supercritical fluids: A review. *Energy* **2014**, *77*, 235−243.

(4) Savage, P. E.; Gopalan, S.; Mizan, T. I.; Martino, C. J.; Brock, E. E. Reactions at Supercritical Conditions: Applications and Fundamentals. *AIChE J.* **1995**, *41*, 1723−1778.

(5) Yu, J.; Eser, S. Thermal Decomposition of Jet Fuel Model Compounds under Near-Critical and Supercritical Conditions. 1. *n*-Butylbenzene and *n*-Butylcyclohexane. *Ind. Eng. Chem. Res.* **1998**, *37*, 4591−4600.

(6) Edwards, T. Cracking and Deposition Behavior of Supercritical Hydrocarbon Aviation Fuels. *Combust. Sci. Technol.* **2006**, *178*, 307−334.

(7) Gudiyella, S.; Buras, Z. J.; Chu, T. C.; Lengyel, I.; Pannala, S.; Green, W.H. Modeling Study of High Temperature Pyrolysis of Natural Gas. *Ind. Eng. Chem. Res.* **2018**, *57*, 7404−7420.

(8) Bolmatov, D.; Brazhkin, V. V.; Trachenko, K. Thermodynamic behaviour of supercritical matter. *Nat. Commun.* **2013**, *4*, No. 2331.

(9) Nishikawa, K.; Morita, T. Inhomogeneity of molecular distribution in supercritical fluids. *Chem. Phys. Lett.* **2000**, *316*, 238−242.

(10) Kajimoto, O. Solvation in Supercritical Fluids: Its Effects on Energy Transfer and Chemical Reactions. *Chem. Rev.* **1999**, *99*, 355−389.

(11) Wu, B. C.; Michael, T. K.; Sandler, S. I. Solvent Effects on Reactions in Supercritical Fluids. *Ind. Eng. Chem. Res.* **1991**, *30*, 822−828.

(12) Tanko, J. M.; Pacut, R. Enhanced Cage Effects in Supercritical Fluid Solvents. The Behavior of Diffusive and Geminate Caged-Pairs in Supercritical Carbon Dioxide. *J. Am. Chem. Soc.* **2000**, *123*, 5703−5709.

(13) Hoijemberg, P. A.; Zerbs, J.; Japas, M. L.; Chesta, C. A.; Schroeder, J.; Aramendía, P. F. Cage Effect in Supercritical Fluids and Compressed Gases in the Photolysis of an Asymmetrically Substituted Diazene. *J. Phys. Chem. A* **2009**, *113*, 5289−5295.
(14) Tucker, S. C.; Maddox, M. W. The Effect of Solvent Density Inhomogeneities on Solute Dynamics in Supercritical Fluids: A Theoretical Perspective. *J. Phys. Chem. B* **1998**, *102*, 2437−2453.
(15) Yoon, T. J.; Ha, M. Y.; Lee, W. B.; Lee, Y. W. Monte Carlo simulations on the local density inhomogeneities of sub- and supercritical carbon dioxide: Statistical analysis based on the Voronoi tessellation. *J. Supercrit. Fluids* **2017**, *119*, 36−43.
(16) Yoon, T. J.; Ha, M. Y.; Lee, W. B.; Lee, Y.W. Molecular dynamics simulation on the local density distribution and solvation structure of supercritical CO_2 around naphthalene. *J. Supercrit. Fluids* **2017**, *130*, 364−372.
(17) Ha, M. Y.; Yoon, T. J.; Tlusty, T.; Jho, Y.; Lee, W. B. Widom Delta of Supercritical Gas-Liquid Coexistence. *J. Phys. Chem. Lett.* **2018**, *9*, 1734−1738.
(18) Ha, M. Y.; Yoon, T. J.; Tlusty, T.; Jho, Y.; Lee, W. B. Universality, Scaling, and Collapse in Supercritical Fluids. *J. Phys. Chem. Lett.* **2020**, *11*, 451−455.
(19) Wang, Z.; Cheng, Z.; Yuan, W.; Cai, J.; Zhang, L.; Zhang, F.; Qi, F.; Wang, J. An experimental and kinetic modeling study of cyclohexane pyrolysis at low pressure. *Combust. Flame* **2012**, *159*, 2243−2253.
(20) Wang, Z.; Ye, L.; Yuan, W.; Zhang, L.; Wang, Y.; Cheng, Z.; Zhang, F.; Qi, F. Experimental and kinetic modeling study on methylcyclohexane pyrolysis and combustion. *Combust. Flame* **2014**, *161*, 84−100.
(21) DeBlase, A. F.; Bruening, C. R.; Lewis, W. K.; Bunker, C. E. In Situ Diagnostic of Supercritical Fuel Surrogates: Probing Heterogeneous Catalysis by Collision-Induced Dissociation in a Molecular Beam Tandem Mass Spectrometer. *Energy Fuels* **2019**, *33*, 10861−10867.
(22) Bunker, C. E.; DeBlase, A. F.; Youtsler, T. A.; Sanders, N. L.; Lewis, W. K. Enhanced Bimolecular Reaction in a Two-Component Fluid under Pyrolytic Conditions: In Situ Probing of the Pyrolysis of Jet Fuel Surrogates Using a Supersonic Expansion Molecular Beam Mass Spectrometer. *Energy Fuels* **2018**, *32*, 3391−3398.
(23) DeBlase, A. F.; Bruening, C. R.; Lewis, W. K.; Bunker, C. E. Probing the Supercritical Pyrolysis Regime by Mass Spectrometry: The Effects of Aliphatic versus Aromatic Content on the Composition of an Endothermic Fuel. *Energy Fuels* **2018**, *32*, 12289−12297.
(24) Senftle, T. P.; Hong, S.; Islam, M. M.; Kylasa, S. B.; Zheng, Y.; Shin, Y. K.; Junkermeier, C.; Engel-Herbert, R.; Janik, M. J.; Aktulga, H. M.; Verstraelen, T.; Grama, A.; van Duin, A. C. T. The ReaxFF reactive force-field: development, applications and future directions. *npj Comput. Mater.* **2016**, *2*, 15011.
(25) Han, Y.; Ma, T. Z.; Chen, F.; Li, W.; Zhang, J.L. Supercritical water gasification of naphthalene over iron oxide catalyst: A ReaxFF molecular dynamics study. *Int. J. Hydrogen Energy* **2019**, *44*, 30486−30498.
(26) Ashraf, C.; Shabnam, S.; Jain, A.; Xuan, Y.; van Duin, A. C. T. Pyrolysis of binary fuel mixtures at supercritical conditions: A ReaxFF molecular dynamics study. *Fuel* **2019**, *235*, 194−207.
(27) Li, G.; Lu, Y.; Qi, S. Investigation of hydrogen oxidation in supercritical H_2O/CO_2 mixtures using ReaxFF molecular dynamics simulation. *J. Supercrit. Fluids* **2020**, *155*, No. 104661.
(28) Dasgupta, N.; Shin, Y. K.; Fedkin, M. V.; van Duin, A. ReaxFF molecular dynamics simulations of electrolyte-water systems at supercritical temperature. *J. Chem. Phys.* **2020**, *152*, No. 204502.
(29) Cheng, T.; Jaramillo-Botero, A.; Goddard, W. A., III; Sun, H. Adaptive accelerated ReaxFF reactive dynamics with validation from simulating hydrogen combustion. *J. Am. Chem. Soc.* **2014**, *136*, 9434−9442.
(30) Bal, K. M.; Neyts, E. C. Merging metadynamics into hyperdynamics: accelerated molecular simulations reaching time scales from microseconds to seconds. *J. Chem. Theory Comput.* **2015**, *11*, 4545−4554.
(31) Bal, K. M.; Neyts, E. C. Direct observation of realistic-temperature fuel combustion mechanisms in atomistic simulations. *Chem. Sci.* **2016**, *7*, 5280−5286.
(32) Jia, Z.; Huang, H.; Zhou, W.; Qi, F.; Zeng, M. Experimental and Modeling Investigation of *n*-Decane Pyrolysis at Supercritical Pressures. *Energy Fuels* **2014**, *28*, 6019−6028.
(33) Wang, Y.; Jiang, P. X.; Zhu, Y. A novel global reaction modeling approach considering the effects of pressure on pyrolysis of *n*-decane at supercritical pressures. *Fuel* **2021**, *287*, No. 119416.
(34) Wang, H.; Gong, S.; Liu, G. Atmospheric and high pressures pyrolysis study of *n*-decane in a flow reactor with online GC-MS/FID analysis: Experiments and modeling. *J. Anal. Appl. Pyrolysis* **2021**, *155*, No. 105065.
(35) Plimpton, S. Fast Parallel Algorithms for Short-Range Molecular Dynamics. *J. Comput. Phys.* **1995**, *117*, 1−19.
(36) Thompson, A. P.; Aktulga, H. M.; Berger, R.; Bolintineanu, D. S.; Brown, W. M.; Crozier, P. S.; in 't Veld, P. J.; Kohlmeyer, A.; Moore, S. G.; Nguyen, T. D.; Shan, R.; Stevens, M. J.; Tranchida, J.; Trott, C.; Plimpton, S. J. LAMMPS - a flexible simulation tool for particle-based materials modeling at the atomic, meso, and continuum scales. *Comput. Phys. Commun.* **2022**, *271*, No. 108171.
(37) Chen, C.; Jiang, X.; Sui, Y. Prediction of transport properties of fuels in supercritical conditions by molecular dynamics simulation. *Energy Procedia* **2019**, *158*, 1700−1705.
(38) Jorgensen, William L.; Maxwell, David S.; Tirado-Rives, J. Development and Testing of the OPLS All-Atom Force Field on Conformational Energetics and Properties of Organic Liquids. *J. Am. Chem. Soc.* **1996**, *118*, 11225−11236.
(39) Wang, Y.; Gong, S.; Li, L.; Liu, G. Sub-to-supercritical properties and inhomogeneity of JP-10 using molecular dynamics simulation. *Fuel* **2021**, *288*, No. 119696.
(40) Te Velde, G.; Bickelhaupt, F. M.; Baerends, E. J.; Fonseca Guerra, C.; Van Gisbergen, S. J. A.; Snijders, J. G.; Ziegler, T. Chemistry with ADF. *J. Comput. Chem.* **2001**, *22*, 931−967.
(41) Ashraf, C.; van Duin, A. C. T. Extension of the ReaxFF Combustion Force Field toward Syngas Combustion and Initial Oxidation Kinetics. *J. Phys. Chem. A* **2017**, *121*, 1051−1068.
(42) Arvelos, S.; Abrahão, O.; Eponina Hori, C. ReaxFF molecular dynamics study on the pyrolysis process of cyclohexanone. *J. Anal. Appl. Pyrolysis* **2019**, *141*, No. 104620.
(43) Liu, H.; Liang, J.; He, R.; Li, X.; Zheng, M.; Ren, C.; An, G.; Xu, X.; Zheng, Z. Overall mechanism of JP-10 pyrolysis unraveled by large-scale reactive molecular dynamics simulation. *Combust. Flame* **2022**, *237*, No. 111865.
(44) Chenoweth, K.; van Duin, A. C. T.; Goddard, W. A., III ReaxFF Reactive Force Field for Molecular Dynamics Simulations of Hydrocarbon Oxidation. *J. Phys. Chem. A* **2008**, *112*, 1040−1053.
(45) Zeng, J.; Cao, L.; Chin, C. H.; Ren, H.; Zhang, J. Z. H.; Zhu, T. ReacNetGenerator: an automatic reaction network generator for reactive molecular dynamics simulations. *Phys. Chem. Chem. Phys.* **2020**, *22*, 683−691.
(46) Rycroft, C. H. VORO++: a three-dimensional voronoi cell library in C++. *Chaos* **2009**, *19*, No. 041111.
(47) Malewicki, T.; Brezinsky, K. Experimental and modeling study on the pyrolysis and oxidation of n-decane and n-dodecane. *Proc. Combust. Inst.* **2013**, *34*, 361−368.
(48) Cavallotti, C.; Pelucchi, M.; Frassoldati, A. Analysis of acetic acid gas phase reactivity: Rate constant estimation and kinetic simulations. *Proc. Combust. Inst.* **2019**, *37*, 539−546.
(49) Christopher E., Bunker; Harry W., Rollins; Sun, Y., *Supercritical Fluid Techonology in Chemical Engerineering: Syntheses: Properties, and Applications*; CRC Press: New York, 2002.

https://doi.org/10.1021/jacsau.2c00359
JACS Au 2022, 2, 2081−2088